International Journal of Concrete Structures and Materials

RESEARCH

Open Access

Interfacial Shear Behavior of Composite Concrete Substrate to High-Performance Concrete Overly After Exposure to Elevated Temperature

Nagat M. Zalhaf[1], Sabry Fayed[1] and Mohamed H. Zakaria[1*]

Abstract

Basically, the interface shear strength between two concrete layers of varying ages must be sufficient to withstand the applied actions on the structure, specifically fire attack, which may cause the complete collapse of the composite structure. Thus, interfacial shear behavior was investigated and analyzed in this paper under the influence of a set of parameters, including temperature (25, 200, 400, and 600 °C), time exposure (30, 60, 90, 120, and 180 min), concrete type, and fibers type (polypropylene fiber (PPF), steel fiber (SF), and hybrid fiber) by employing a Z-shape push-off test. The test consists of two parts with different ages: normal strength concrete (NCS) and high-performance concrete (HPC). HPC includes high-strength concrete (HSC) and fly ash concrete (FAC). Initially, twenty-five Z-shaped push-off tests were made, four of which were cast as one unit (NSC/or concrete with hybrid (FSP)), and the rest were composite specimens. Furthermore, a 3D finite element model of a composite push-off specimen was developed to simulate and analyze the impact of various time and temperature exposures on the interfacial shear strength of composite specimen N-FSP. The results indicated that temperature degree and exposure time adversely affected the interfacial shear strength. Also, interfacial shear strength is significantly influenced by fiber types. Including combined fiber (SF + PPF) improved the interfacial shear strength by 114% compared to the composite specimen NSC-NSC after exposure to a temperature of 600 °C. In contrast, using PPF negatively affected the interfacial shear strength, recording only 84% of the composite specimen NSC-NSC. In addition, the inclusion of supplementary cementitious material enhanced the interfacial shear strength by 60.5% in the NSC-FAC composite specimen with 30% FA, compared to the NSC-NSC specimen. Finally, a finite element (FE) model was proposed with a satisfactory level of accuracy (0.95 to 1.03) in predicting the maximum shear strength. Additionally, the difference between the FE and experimental stiffness was between 0.92 and 1.07.

Keywords Interfacial shear strength, High-performance concrete, Elevated temperature, 3D finite element models

1 Introduction

Over the last several years, researchers have focused heavily on developing innovative repair techniques and materials for reinforced concrete (RC) structures. One of the traditional repair techniques is rehabilitation, which involves placing a new concrete layer on the existing one (Santos & Julio, 2007). Usually, the concrete-to-concrete interface between two concrete layers cast at different ages is the weakest area of the

Journal information: ISSN 1976-0485 / eISSN 2234-1315.

*Correspondence:
Mohamed H. Zakaria
mohammed_hamed@eng.kfs.edu.eg
[1] Department of Civil Engineering, Faculty of Engineering, Kafrelsheikh University, Kafr El-Shaikh 33511, Egypt

concrete structure. To ensure the reliable functioning of these connections, a quantifiable amount of shear strength at the interface must be mobilized (Julio et al., 2004). The impact of monotonic loading on the strength of concrete-to-concrete interface bonds has been the focus of a number of investigations (Bentz et al., 2018; Beushausen, 2010; Feng et al., 2020; Mansour & Fayed, 2021; Park & Kim, 2021; Santos et al., 2012; Tayeh et al., 2013; Valikhani et al., 2021). As a result of these studies, the primary mechanisms for shear transfer between concrete layers cast at varying ages may be identified: adhesion, friction, and dowel action. Moreover, the shear transfer stress depends on many variables including concrete substrate surface preparation (Feng et al., 2020; Tayeh et al., 2013), overlay concrete strength (Mansour & Fayed, 2021; Santos et al., 2012), bond agent (Park & Kim, 2021), shear connectors between the two concrete layers (Valikhani et al., 2021), moisture condition of the existing concrete layer at the time of casting (Bentz et al., 2018; Beushausen, 2010), fiber reinforcement type of the concrete overlay (Zanotti et al., 2018).

In the case of fire, horizontal cracks have been formed at the interface between the concrete layers under fire load in some studies (Ghazy et al., 2023). In contrast, others observed no crack propagating at the interface Baloch et al. (Baloch et al., 2023). According to Ghazy et al. (2023), the concrete type, strengthening side, connection type, and fire direction significantly affected the load–deflection curves of the composite slabs after fire exposure. Thus, studying the shear transfer stress between two concrete layers after exposure to elevated temperatures is essential for understanding composite structures' overall behavior under elevated temperatures.

Through the employment of slant shear, push-off, and splitting tensile tests, several researchers have experimentally examined the concrete-to-concrete interface bond at elevated temperatures (Abo Sabah et al., 2019; Gao et al., 2019; Haido et al., 2021; Sun et al., 2022). The findings show that the interface bond strength considerably decreased as the temperature increased. This is due to the deterioration of the cement paste under elevated temperature, the difference in thermal expansion between cement paste and aggregate, micro-cracks were developed, consequently, deterioration in the interface bond strength. In slant shear tests, positive correlations were observed between the maximum shear strength and the shear angle; larger shear angles corresponded to greater shear strengths. Sun et al. (Sun et al., 2022) concluded that the maximum shear strength after exposure to a temperature of 700 was 40%, 50%, and 57% of that at 100 °C for shear angles 30 °C, 38 °C, and 45 °C, respectively.

Regarding shear strength at the interface during a fire, surface preparation of the concrete is crucial. According to Chen et al. (Chen et al., 2023), after being exposed to an elevated temperature of 200 °C, the smooth surface only maintained 20–35% of its shear strength at room temperature, while the rough surface retained approximately 65–87.5% of its shear strength at room temperature for the same condition. In contrast, Shang et al. (2021) revealed that the surface roughness adversely affected the shear strength when the surface roughness was higher than 3.5 mm.

Regarding existing fiber in the overlay concrete, Goa et al. (2019) experimentally studied the bond strength of the concrete-to-concrete interface after exposure to elevated temperatures through conducted slant shear tests. The parameters include overlay concrete types, NSC or engineering cementitious composite (ECC), and scenario of fire effect; the first scenario, the concrete substrate subjected to temperature up to 800 °C, then repaired with overlay concrete, while the second scenario, the concrete substrate repaired with concrete overlay then exposed to elevated temperature up to 800 °C. Their results indicated that the utilized composite NSC/ECC observed higher bond strength than NSC/NSC. Furthermore, the bond strength improved with increasing temperature up to 200 °C; the bond strength gradually decreased with temperature increase. Shang et al. (2021) conducted a push-off test on a concrete substrate heated up to 800 °C and strengthened with engineered cementitious composite reinforced with polyethylene (PE-ECC) or polyvinyl alcohol (PVA-ECC) fibers. The results showed that the PVA-ECC specimen recorded a shear strength of 2.27 MPa with an increasing ratio of 17.6% as compared to the PVA-ECC specimen after exposure to 600 °C. In addition, concrete type plays an essential role in the interface shear strength. Chen et al. (2023) indicated that the inclusion of high-strength concrete can improve the interface shear strength and depend on the concrete substrate strength, where existing HSC in the two interface sides led to an increase in the shear strength by 119% as compared to use normal strength concrete in the two-interface side. Moreover, the bond agent had an evident effect on the bond strength at ambient and elevated temperatures. Chen et al. (2023) determined that using cement mortar at the interface between two NSC layers can improve the shear strength by 40%, 32%, and 119% at 20 °C, 200 °C, and 600 °C, respectively, as comparison without a bond agent.

High-performance concrete (HPC) is one of the traditional repair materials for RC structures due to its high mechanical properties and durability (Khaliq & Kodur, 2011). From previous studies (Babalola et al., 2021; Ghazy et al., 2022; Khaliq & Kodur, 2011; Poon et al., 2001),

existing 30% fly ash (FA) can improve the mechanical properties of concrete after exposure to elevated temperature. Moreover, adding steel fiber (SF) and polypropylene fiber (PPF) has a significant effect in enhancing the mechanical properties at high temperatures (Algourdin et al., 2020; Ghazy et al., 2022; Khaliq & Kodur, 2011; Li & Liu, 2016). Furthermore, the use of HPC can improve the post-fire behavior of RC members (Baloch et al., 2023; Ghazy et al., 2023; Khaliq & Kodur, 2013).

However, limited papers focus on the Z shape push-off test of different concrete cast at different ages after exposure to elevated temperature (Chen et al., 2023; Shang et al., 2021). Thus, this investigation aims to study the interface shear strength at ambient temperature or after exposure to elevated temperature through the Z-shape push-off test. Firstly, the authors examined the effect of different temperatures 25, 200, 400, and 600 on the interface shear strength for Z specimen cast with NSC and fly ash concrete containing hybrid fiber (0.5% SF + 0.5% PPF) (N-FSP). Also, studying the interfacial shear behavior of N-FSP specimens heated to temperatures of 600 °C for 30, 60, 90, 120, and 180 min. Secondly, from the first stage, the temperature of 600 °C and 90 min exposure time were selected to investigate the effect of concrete types and fiber types on the interfacial shear behavior at ambient and after exposure to elevated temperatures. The results were compared to monolithic NSC and FSP specimens. Accordingly, the results of this study will assist engineers in comprehending the behavior of RC members enhanced with HPC in a high-temperature environment. In addition, the data obtained from this study can be used to validate finite element models of composite RC members under fire exposure conditions.

2 Experimental Work

2.1 Material

A Z-shape push-off test consists of two parts: normal strength concrete (NCS) and high-performance concrete (HPC). Concrete mixtures have been prepared using ordinary Portland cement (CEM 42.5), crushed limestone with a maximum nominal size of 10 mm, river sand, water, and polycarboxylate superplasticizer. HPC includes high-strength concrete (HSC), fly ash concrete (FAC) by replacing 30% of cement with FA type F, FAC with 0.5% polypropylene fiber (PPF), 0.5% steel fiber (SF), and hybrid fiber (0.5% PPF + 0.5% SF). Fig. 1 presents the fibers employed in this study. Table 1 displays aggregate characteristics, whereas Tables 2 and 3 highlight fiber characteristics. The components of concrete mixtures are given in Table 4.

Where HRWR refer to high-range water reducers, FA: fly ash SF: steel fiber, and PPF: polypropylene fibers.

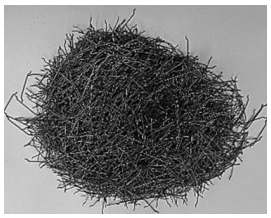

a) Steel fibers

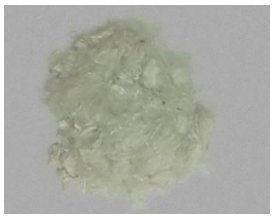

b) Polypropylene fibers

Fig. 1 Types of the used fibers

2.2 Specimen Perpetration

The interfacial shear strength of HPC and NSC cast at various ages at ambient temperature and after exposure to elevated temperature was investigated by making and testing a total of 25 Z-shaped push-off tests. The Z-shape specimen dimensions were $100 \times 200 \times 400$ mm, where the interface area was 100×160 mm^2. To prevent edge failures brought on by potential flexural loads, the reinforcement rebar with a 10 mm diameter is included. This study used no shear connectors across the interface to demonstrate the pure shear between the two concrete parts. Fig. 2 depicts the specimen dimension and reinforcement details.

The first part of the Z-shape was cast with NSC (N) as the concrete substrate; for studying the effect of concrete type, the second part was cast with NSC specimen (N–N) as reference one and compared with specimen cast with HSC (specimen N–H), FAC (specimen N-F). Specimens that have FAC incorporating 0.5% steel fiber (specimen N-FS), 0.5% polypropylene fiber (specimen N-FP), and hybrid fibers (specimen N-FSP) were considered for studying the influence of fiber types. The following procedures were used to create the composite specimens. (1) Half of the Z-shape was fabricated, reinforcement was placed inside, and then the NSC was cast. (2) After 24 h, the concrete part was demoulded and cured in water for 28 days. (3) According to Fib, the NSC surface was roughened by 1.5 mm to increase the bond strength at the interface (CEB-FIP & Model Code., 2010). Moreover, previous research (Jiang et al., 2020, 2021; Yang et al., 2022; Zhang et al., 2020a, 2020b) had demonstrated that grooved treatment with dimensions varied from 10 to 20 mm significantly enhanced the shear strength, while increasing the space between grooves led to a decrease in the interfacial shear strength. In this study, two grooves with 1.5 cm width and 1 cm depth were fabricated in the NSC surface, as shown in Fig. 3. The surface was cleaned from dust and wetted by spring water. (4) The NSC part was placed into the mold, and HPC was cast; after 24 h, the Z-shape specimen was demoulded and cured in water

Table 1 Physical properties of the aggregates utilized

Properties	Coarse aggregate		Fine aggregate	Specification and reference
	Crushed limestone		River sand	
Bulk specific gravity	–	2.6	2.55	ASTM-C127-01 (2017)
Water absorption ratio	%	1.5%	1%	ASTM C128-01 (2017)
Unit weight	kg/m^3	1500	1560	ASTM-C29 (2010)

Table 2 The chemical, physical, and mechanical properties of the employed cement and FA (according to the manufacturers)

Chemical component (wt.%)	Cement	FA
SiO_2	20.65	60.28
Al_2O_3	4.4	28.59
Fe_2O_3	5.05	4.99
Total $SiO_2 + Al2O_3 + Fe_2O_3$	30.1	93.86
CaO	62.20	2.38
Na_2O	0.38	0.48
MgO	1.90	2.92
Loss on Ignition	1.34	–
Insoluble Residue	0.88	1.1
Physical and mechanical properties		
Specific gravity	3.15	2.3
Specific surface area (cm^2/g)	3500	4500

for 28 days, then the specimens were placed at room temperature of 25 °C for 30 days until the time of heating, to prevent the concrete from becoming too damp, which could cause explosive spalling as mentioned by Ahmad et al. (Ahmad et al., 2020), Ghazy et al. (2023). Fig. 4 shows the steps of casting composite specimens. In addition, four Z-shape specimens were cast as one unit with NSC/or FSP for comparison with the composite specimen at ambient temperature and after exposure to a temperature of 600 °C. Table 5 presents the summary of specimens.

For studying the mechanical properties of concrete mixes at room temperature and after exposure to elevated temperatures, six cubes with dimensions of $\times 1010 \times 10$ cm^3 were cast from each concrete mix for compression test (BS En 12390–3, 2019), while six cylinders have 10 cm diameter and 20 cm height were taken for tensile strength (BS En 12390–6, 2009).

2.3 Heating Stage

After 60 days, the specimens were heated in an electric furnace with dimensions of $500 \times 400 \times 400$ mm. The heating rate was 50 °C/min to simulate the actual fire situation. In the case of studying the temperature effect on the interface shear strength, specimens N-FSP and N–N were heated at 200 °C, 400 °C, and 600 °C, where the specimens were exposed to temperature from all sides, as shown in Fig. 5a. When the furnace reached the target temperature, it stayed for 90 min, after that, the furnace switched off. The specimens cooled down naturally to room temperature. To observe the effect of time exposure on the interface shear strength, specimen N-FSP was exposed to a temperature of 600 °C for different times of 30, 60, 90, 120, and 180 min.

2.4 Loading Test

A direct shear test was conducted using a compression machine with a loading rate of 0.01 kN/sec, as shown in Fig. 5b. The load was recorded automatically, while the displacement was recorded using a digital dial gauge

Table 3 Properties of employed fibers (SF, and PPF) and steel rebars (according to the manufacturers)

Properties	Fibers		Steel reinforcement rebar	
	Steel (SF)	Polypropylene (PPF)	Main reinforcement	Stirrup
Length, (mm)	35	Gradient of 18	–	–
Diameter	0.8 (mm)	18 (μm)	10 mm	8 mm
Specific gravity	7.85	0.91	7.85	7.85
Shape	Hooked end	Fiber mesh	–	
Tensile strength, (Mpa)	≥ 1000	300–400	360	360
Elastic modulus, (Gpa)	210	3.6	210	210
Melting point, (°C)	–	160 °C	–	–

Table 4 Components of various concrete mixtures

Mix ID			NSC	HSC	FAC	FAC-SF	FAC-PP	FAC-(SF + PP)
Component	**Unit**	**Concrete type**	**Normal strength Concrete**	**High strength concrete**	**30% FA**	**30% FA + 0.5% SF**	**30% FA + 0.5%PPF**	**30% FA + 0.5% SF + 0.5%PP**
Cement		kg/m^3	350	550	550	550	550	550
FA			–	–	165	165	165	165
Sand			680	834.7	852.9	843.7	822.9	816.4
Crushed limestone			1020	834.7	852.9	843.7	822.9	816.4
Water			200	176	165	165	176	176
HRWR			–	7.65	4.5	6.75	6.75	12.15
PPF			–	–	–	–	4.5	4.5
SF			–	–	–	39	–	39
Water–binder ratio (W/B)			0.57	0.32	0.3	0.3	0.32	0.32
Compressive strength								
28 day		MPa	35	75	68	64	66	70
600		°C	23.8	39	44.88	44.8	36.3	50
Tensile strength								
28 day		MPa	1.8	5.9	5.5	6.5	6	7
600 °C		°C	0.94	1.9	1.77	3.79	1.29	3.9

(DG). The crack propagation and failure pattern have been observed during the test.

3 Results

3.1 Failure Pattern

After exposure to elevated temperatures, no spalling occurred during the fire test neither under different temperatures nor at different times, except specimen N-FSP which consists of NSC and fly ash concrete with hybrid fibers, showed explosive spalling and contributed to a total collapse of Z-shape push off specimen after exposure to a temperature of 600 °C for 180 min as shown in Fig. 6b. This is due to the fact that steel fibers bridge the cracks and prevent the mitigation of vapor water to the atmosphere as discussed by Algourdin et al. (2020).

Under shear load, none of the specimens showed flexural failure because there was enough flexural (main) steel. Fig. 7 presents the failure pattern for a monolithic specimen cast with NSC/or FAC (SF + PPF). Specimen N showed a brittle failure; the aggregate interlock action caused the failure plane to form along the pastes around the aggregate particles, while SF delayed crack propagation in specimen N-FSP. Alimrani and Balazs (2020) displayed that this is because the SF acts as a bridge over the fractures and increases the interlocking activity at the shear interface. At 600 °C, the degradation in the concrete mechanical properties made the concrete more softening, where the cracks were more obvious, as shown in Fig. 7c, d.

Fig. 8 shows three distinct failure patterns that may be observed in composite specimens depending on the crack propagation. Both Chen et al. (2023) and Shang et al. (2021) highlight that interfacial roughness plays a major role in enhancing the interfacial bond between the two concrete parts after fire exposure. Cohesive failure of the concrete substrate indicated that the full failure occurred in the NSC part, as shown in Fig. 8a. When compared to NSC's tensile strength, this indicates a great interfacial bond. This failure was observed in specimens N-H_{25}, N-H_{600}, N-PF_{25}, N-FS_{25}, N-FS_{600}, N-FSP_{25}, N-FSP_{200}, N-FSP_{400}, N-FSP_{600}, N-FSP_{30min}, N-FSP_{60min}, and N-FSP_{90min}. Mixed failure A: adhesive failure with a fracture in the post-cast concrete that is apparent in composite specimen N-FP_{600} as depicted in Fig. 8b. This is due to the fact that the melting of PPF at a temperature of 160 °C and total evaporation at a temperature of 360 °C resulted in producing additional voids, consequently softening concrete (Ghazy et al., 2022). Mixed failure B means the fracture of both NSC and post-cast concrete adjacent to the interface (Fig. 8c). Table 6 presents the failure pattern for different composite push-off specimens.

3.2 Interfacial Shear Properties

This section discusses the interfacial shear behavior for monolithic and composite push-off specimens at ambient temperature and after exposure to elevated temperature. The output of the test includes maximum interfacial shear strength. τ_{max} and calculated by Eq. 1,

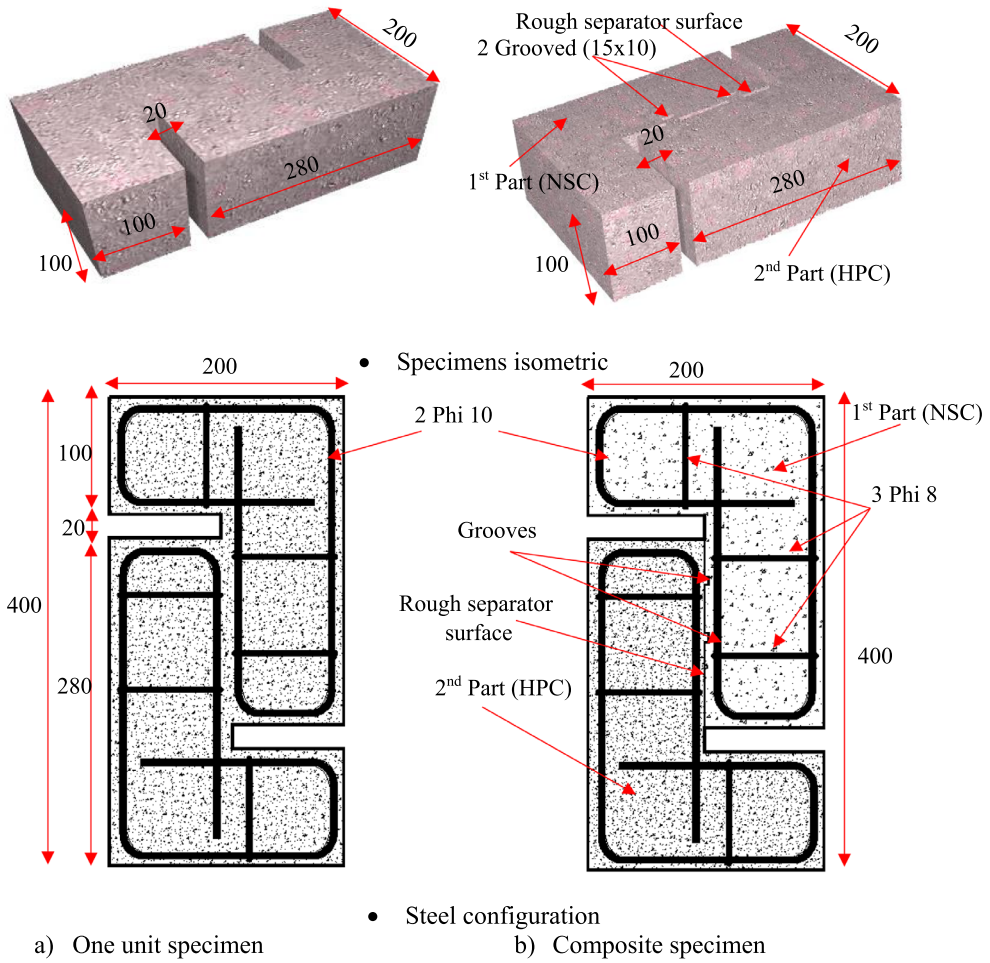

Fig. 2 Specimen dimensions and reinforcement details (all dimensions in mm)

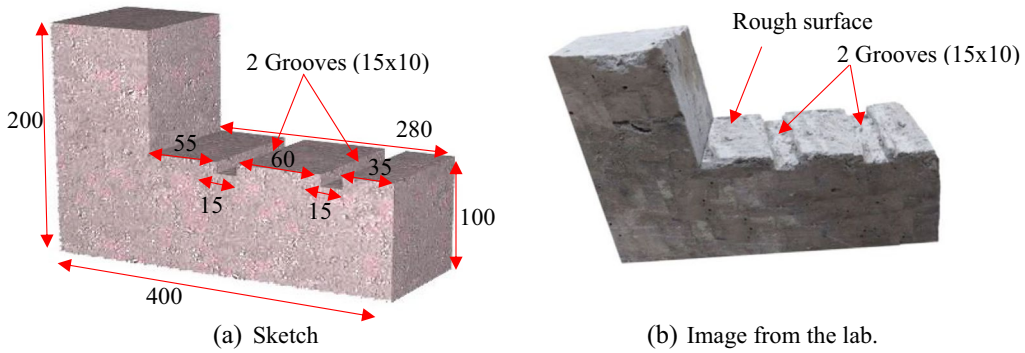

Fig. 3 Grooves arrangement and dimensions (all dimensions in mm)

a) Composite specimen

b) One unit specimen

Fig. 4 Images from specimen perpetration

$$\tau_{max} = \frac{P_{max}}{A} \quad (1)$$

where P_{max} is the maximum vertical load, and A is the interfacial shear area (160×100 mm^2).

Fracture energy is the area under the interfacial shear strength–slip curve, which is calculated by Eq. 2,

$$G = \int_0^{\delta_t^f} \tau d\delta \quad (2)$$

where δ_t^f is the failure slip.

Initial stiffness is the relative maximum shear strength (τ_{max}) to the corresponding slip (δ_t^0) as presented in Eq. 3, according to Sun et al. (2022).

$$K = \frac{\tau_{max}}{\delta_t^0} \quad (3)$$

The effects of different temperatures, different time exposure, concrete type, and fiber type on the interfacial shear characteristics of composite push-off specimens are presented in Table 7 and Figs. 9, 10, 11, 12, and 13.

3.3 Interfacial Shear Load Slip Displacement Curve

Fig. 9 presents the interfacial shear strength versus slip displacement for all specimens at room temperature and after exposure to elevated temperature. For all specimens, the interfacial shear strength–slip curve can be divided into two main parts (Fig. 9). In the first part, the interfacial shear strength increased linearly with a higher rate at a small slip less than 0.05 mm, where the adhesive bond is the main contribution in the interfacial shear strength mentioned by FIB (CEB-FIP, Model Code., 2010). In the second stage, the load increases slowly and, in some cases, becomes constant with a rapid increase in the slip. This behavior can be discussed by: with increasing load, the adhesive bond deteriorates rapidly, and the

Table 5 Details of the investigated specimen

No	Specimen ID	Specimen type	Mix ID	Elevated temperature	
				Time (hour)	Temperature (°C)
1	N25	One unit	NSC	–	–
2	N		NSC	1.5	600
3	FSP25		FAC-(SF + PP)	–	–
4	FSP		FAC-(SF + PP)	1.5	600
5	N-N_{25}	Composite	NC/NC		
6	N-N_{200}		NC/NC	1.5	200
7	N-N_{400}				400
8	N-N_{600}				600
9	H-N_{25}		HSC/NC	–	–
10	H-N_{600}		HSC/NC	1/.5	600
11	F-N_{25}		FAC/NC	–	–
12	F-N_{600}		FAC/NC	1.5	600
13	FS-N_{25}		FAC/NC	–	–
14	FS-N_{600}		FAC/NC	1.5	600
15	FP-N_{25}		FAC/NC	–	–
16	FP-N_{600}		FAC/NC	1.5	600
17	FSP-N_{25}		FAC-(SF + PP)/NC	–	-
18	FSP -N_{200}		FAC-(SF + PP)/NC	1.5	200
19	FSP -N_{400}				400
20	FSP -N_{600}				600
21	FSP –N_{30min}		FAC-(SF + PP)/NC	0.5	600
22	FSP –N_{60min}			1	600
23	FSP –N_{90min}			1.5	600
24	FSP –N_{120}			2	600
25	FSP –N_{180}			3	600

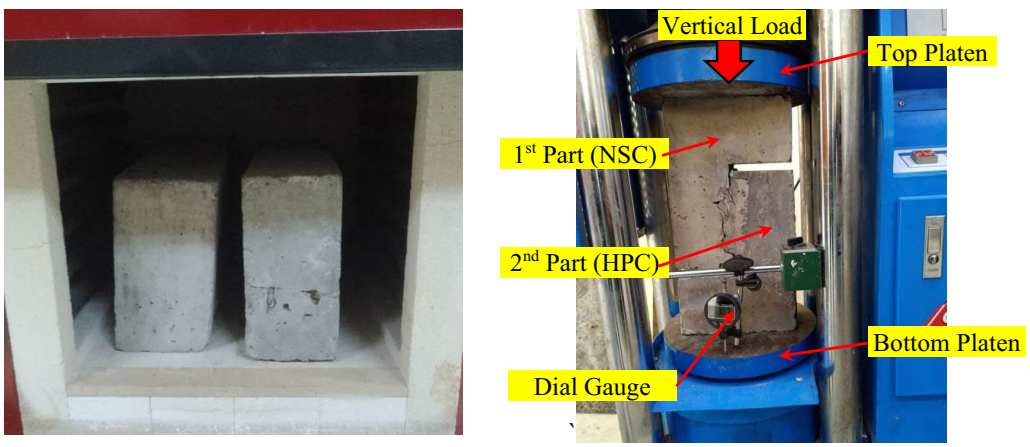

a) Heating stage b) Direct shear test

Fig. 5 Specimen under different loads

a) Specimen after heating stage **b)** Specimen N-FSP after 180 minutes

Fig. 6 Effect of elevated temperature on a specimen

a) N_{25} b) FSP_{25} c) N_{600} d) FSP_{600}

Fig. 7 Crack patterns of monolithic specimen N and FSP

a) Fracture of NSC substrate b) Mixed failure A c) Mixed failure B

Fig. 8 Failure pattern in composite push-off test

shear friction introduced by mechanical interlocking becomes the main load transfer mechanism and resists the slip increase.

Moreover, the temperature degree and temperature time adversely affected the interfacial shear behavior. The maximum shear strength of the specimens decreased; at the same time, the ductility increased except for the specimen exposed to a temperature for 120 min, which recorded the least ductility, as shown in Fig. 9b. In contrast, the effect of concrete type was not obvious at room temperature; the use of fibers can improve the ductility of the specimens. In addition, its effect is more visible after exposure to elevated temperature, where the composite push-off specimens containing SF (N-FSP, N-SF) displayed better behavior than the specimen without SF, as shown in Fig. 9f. In contrast, the specimen included PPF showed brittle behavior after exposure to elevated temperature. It should be noticed that the

Table 6 Failure pattern for different composite push-off specimens

No	Specimen ID	Specimen type	Mix ID	Failure pattern
1	N25	One unit	NSC	–
2	N		NSC	–
3	FSP25		FAC-(SF + PP)	–
4	FSP		FAC-(SF + PP)	–
5	N-N_{25}	Composite	NC/NC	Mixed failure B
6	N-N_{200}		NC/NC	Mixed failure B
7	N-N_{400}			Mixed failure B
8	N-N_{600}			Mixed failure B
9	H-N_{25}		HSC/NC	Fracture of NSC
10	H-N_{600}		HSC/NC	Fracture of NSC
11	F-N_{25}		FAC/NC	Mixed failure B
12	F-N_{600}		FAC/NC	Fracture of NSC
13	FS-N_{25}		FAC/NC	Fracture of NSC
14	FS-N_{600}		FAC/NC	Fracture of NSC
15	FP-N_{25}		FAC/NC	Fracture of NSC
16	FP-N_{600}		FAC/NC	Mixed failure A
17	FSP-N_{25}		FAC-(SF + PP) /NC	Fracture of NSC
18	FSP -N_{200}		FAC-(SF + PP) /NC	Fracture of NSC
19	FSP -N_{400}			Fracture of NSC
20	FSP -N_{600}			Fracture of NSC
21	FSP –N_{30min}		FAC-(SF + PP) /NC	Fracture of NSC
22	FSP –N_{60min}			Fracture of NSC
23	FSP –N_{90min}			Fracture of NSC
24	FSP –N_{120}			Mixed failure B
25	FSP –N_{180}			Spalling

Table 7 Interfacial shear properties of push-off specimens

Specimen ID	τ_{max}(MPa)	K (N/mm^3)	G (N/mm)
N_{25}	3.5	18	0.35
N_{600}	1.39	11.6	0.14
FSP_{25}	5.62	23.4	3.5
FSP_{600}	3.63	13.67	1.42
N-N_{25}	2.41	13.4	0.58
N-N_{200}	2.28	11.66	0.42
N-N_{400}	1.4	9.59	0.19
N-N_{600}	1.14	10.8	0.08
H-N_{25}	2.77	15.09	0.59
H-N_{600}	1.36	7.77	0.18
F-N_{25}	2.88	16.76	0.57
F-N_{600}	1.83	9.58	0.32
FS-N_{25}	2.68	14.25	0.98
FS-N_{600}	2.06	10.96	0.74
FP-N_{25}	2.9	15.18	1.00
FP-N_{600}	1.03	6.87	0.11
FSP-N_{25}	3	14.90	0.99
FSP-N_{200}	2.9	11.56	1.1
FSP-N_{400}	2.68	10.68	1.12
FSP-N_{600}	2.44	8.91	1.14
FSP-N_{30min}	2.68	12.25	1.02
FSP-N_{60min}	2.74	11.58	1.06
FSP-N_{90min}	2.45	8.91	1.14
FSP-N_{120min}	1.4	5.88	0.36
FSP –N_{180min}	0	0	0

interfacial shear strength–slip curve for monolithic specimens N and FSP was stiffer and recorded higher shear strength as compared to composite specimens, as shown in Fig. 9c–f. This is due to the adhesion between cement paste and aggregates, mechanical interlocking of aggregates, and SF at the interfacial shear zone, which delay cracks propagation.

3.4 Effect of Temperature

The interfacial shear strength of composite push-off specimens N–N and N-FSP at different temperature exposures up to 600 °C are presented in Fig. 10. The output results indicated that specimen N-FSP showed better performance than specimen N–N at ambient and after elevated temperature. The interfacial shear strength of specimen N–N decreased rapidly with increasing temperature up to 400 °C, where the remained residual shear strength at 400 was 54% of that at ambient temperature. After 400 °C, the rate of deterioration in the residual interfacial shear strength decreased to a record 44% after exposure to a temperature of 600 °C. This significant deterioration can be explained by the evaporation of free and bond water at 100 °C Babalola et al. (Babalola et al., 2021), dehydration of C-S-H at 560 °C, the mismatch in the thermal expansion of cement paste and aggregate, which create micro-cracks at interfacial transition zone Ma et al. (Ma et al., 2015). These cracks weaken the aggregate interlocking Schneider (Schneider, 1988). Whereas the interfacial shear strength of specimen N-FSP decreased gradually with increasing temperature, the shear strength was about 96.6%, 89.3%, and 81.3% of that at ambient temperature for 200, 400, and 600 °C. The results are relevant to Abo Sabah et al. (Abo Sabah et al., 2019). This improvement is due to the increase in the temperature up to 200 °C made as autoclave and accelerated the hydration process of the anhydrate cement and FA particles at the interfacial zone and produced additional silicate hydrate gel, which filled the void in this area and consequently increase adhesion as observed by Gao et al. (2019) and Ghazy et al. (2022). In general, the residual interfacial shear strength of specimen N-FSP was 9%, 25%, 87.5%, and 114% higher compared to specimen N–N at temperatures of 25, 200, 400, and 600 °C, respectively. This increase was because SF plays an evident role

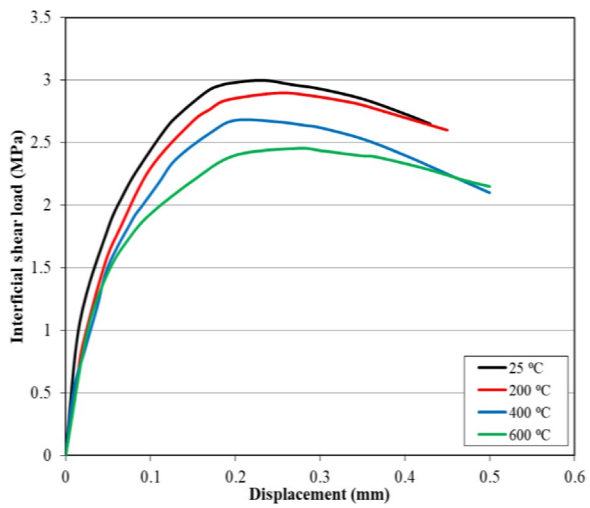

a) Effect of temperature

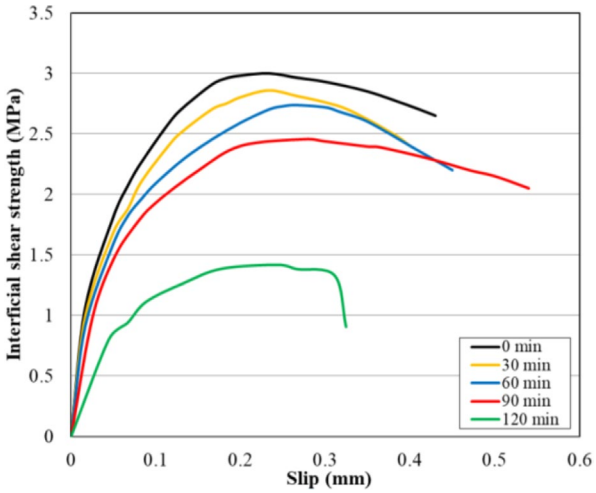

b) Effect of temperature time

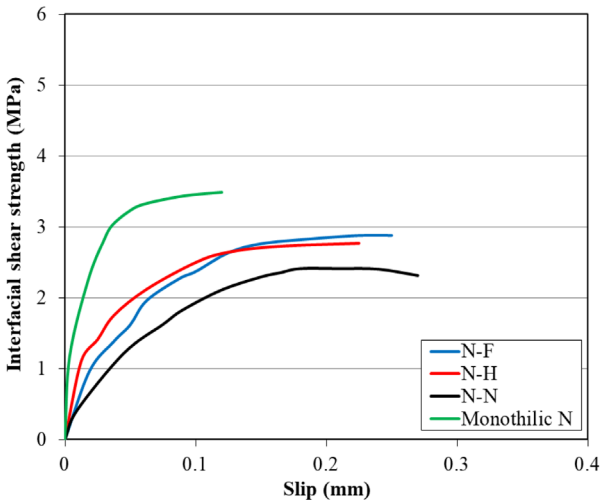

c) Effect of concrete types at 25 ºC

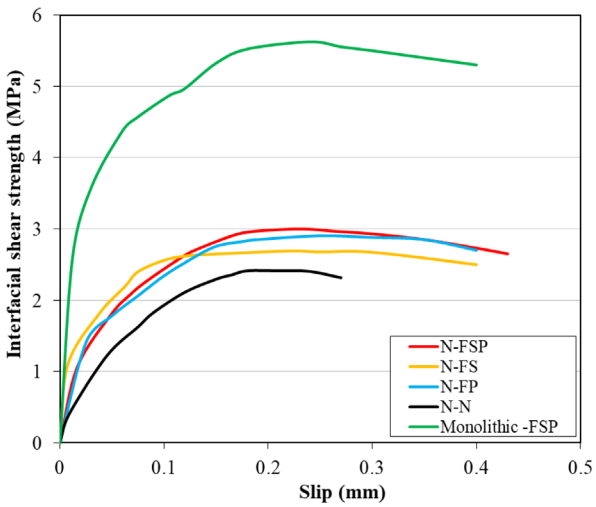

d) Effect of fiber types at 25 ºC

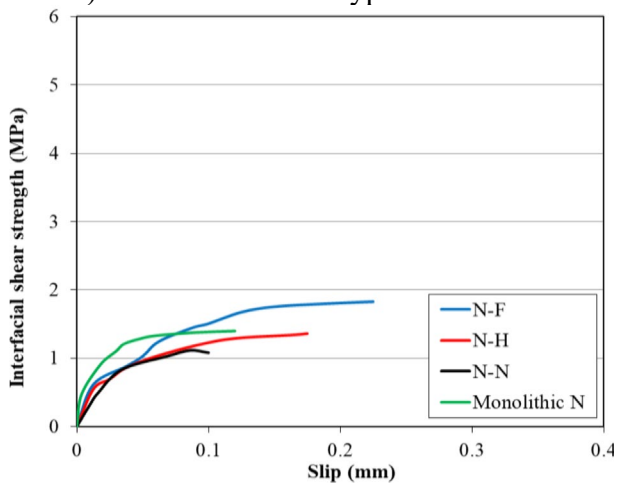

e) Effect of concrete types at 600 ºC

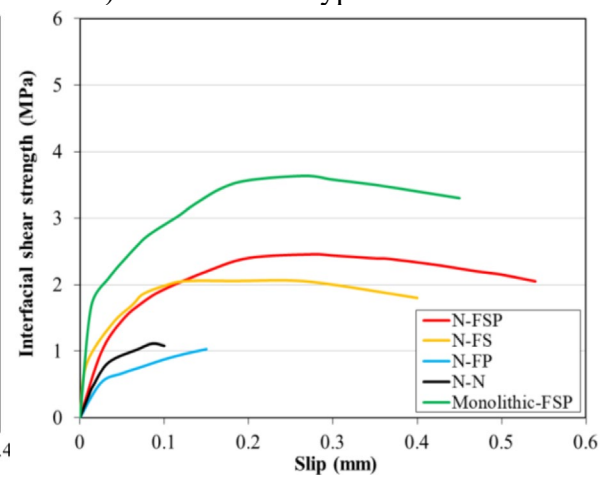

f) Effect of fiber types at 600 ºC

Fig. 9 Interfacial shear strength–slip displacement curve

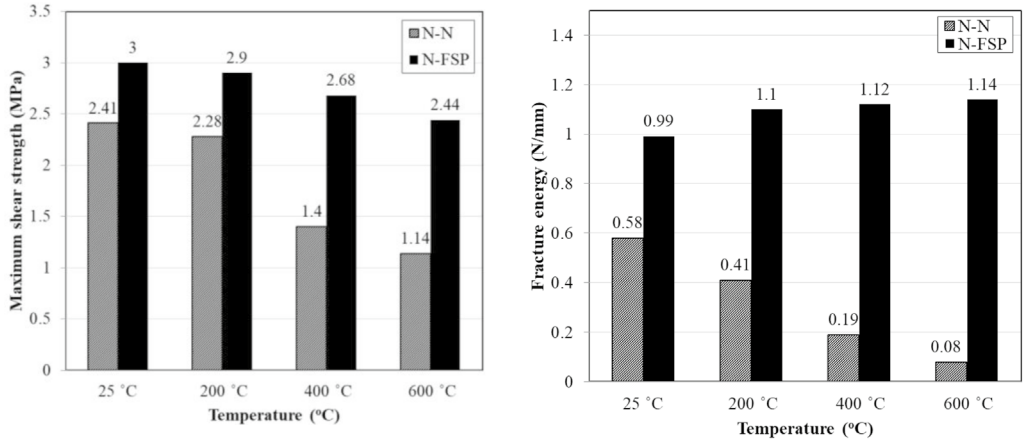

a) Shear strength b) Fracture energy

Fig. 10 Effect of elevated temperature on the residual interfacial shear strength

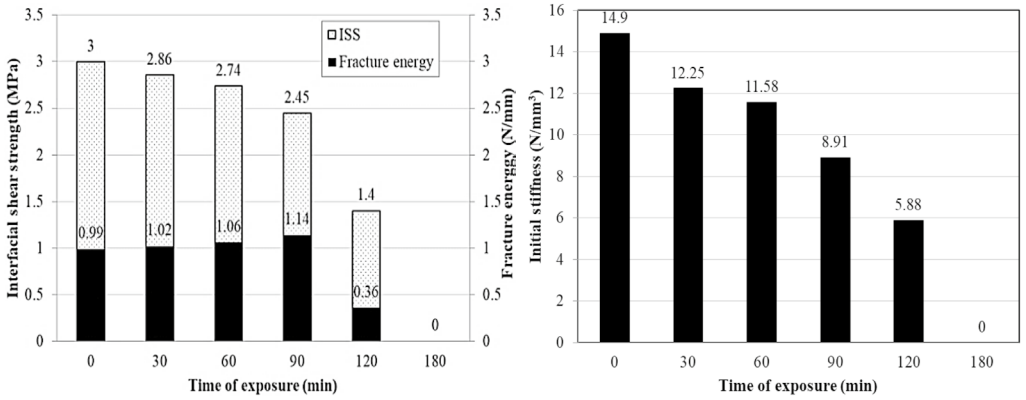

a) Shear strength, fracture energy b) Stiffness

Fig. 11 Effect of time exposure on the interfacial shear properties of composite specimen N-FSP

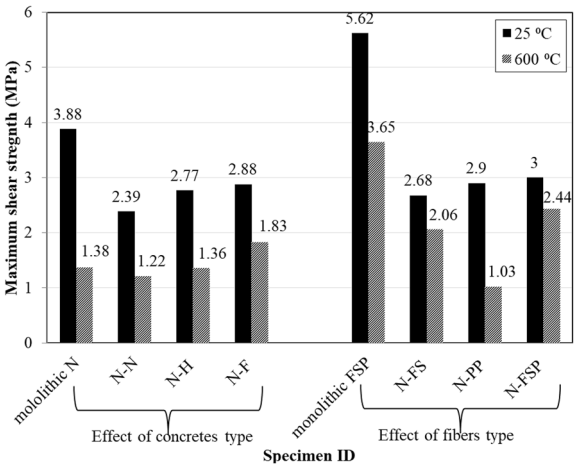

Fig. 12 Maximum shear strength of different specimens after 600 °C

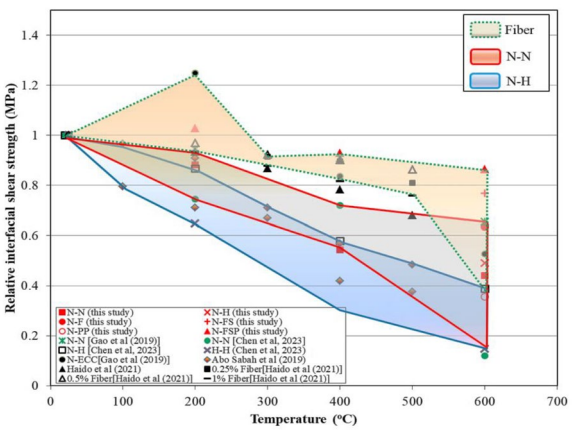

Fig. 13 The relative interfacial shear strength of roughness surface at elevated temperature

in bridging the crack Shang et al. (Shang et al., 2021) and increasing the mechanical interlocking Alimrani and Balazs (Alimrani & Balazs, 2020). Moreover, Fig. 10b indicates that specimen N-FSP confirmed a slight increase in the fracture energy with increasing temperature and recorded an increase of 15% after exposure to a temperature of 600 °C, while specimen N–N exhibits a significant decrease in the fracture energy. This behavior proved the significant role of using SF fiber in enhancing the ductility of the specimen after exposure to elevated temperature.

3.5 Effect of Time Exposure

The composite push-off specimen N-FSP was used to study the effect of different time exposures of 30, 60, 90, 120, and 180 min at a temperature of 600 °C on the residual interfacial shear properties, as depicted in Fig. 11. From the results, it can be noticed that by increasing time of exposure the specimen N-FSP exhibits degradation in its interfacial shear strength with slow rate up to 90 min, the interfacial shear strength was 95%, 91%, 81.3% of the initial shear strength at room temperature for 30, 60 and 90 min. The results agree with Mathews et al. (2021). After 90 min, the shear strength decreased sharply to nearly 50% of that at room temperature. Because increasing exposure time results in microcracks, the concrete becomes softer and loses its mechanical properties. The same trend was observed in the initial stiffness, which recorded 82%, 77.7%, 59.7%, and 39.5% of the initial stiffness at room temperature for 30, 60, 90, and 120 min, respectively. This proved that the concrete mechanical properties at the interface influence the interfacial shear performance. On the other hand, the fracture energy observed marginally increases with a time increase up to 90 min to reach 15% higher than that of the initial temperature. At 120 min, the specimen was softer and brittle, significantly deteriorating the shear strength behavior. After exposure to a temperature of 600 for 180 min, the specimen showed explosive spalling. This is attributed to the SF bridging the cracks and preventing escaping water evaporation, as motioned before Algourdin et al. (2020).

3.6 Effect of Concrete Type

Specimens N–N, N–H, and N-F were used to observe the effect of concrete type on the interfacial shear strength after exposure to an elevated temperature of 600 °C for 90 min; the interfacial shear strength was plotted in Fig. 12. From the results, it can be observed that the concrete type has a significant effect on the interfacial shear strength at ambient temperature and after exposure to elevated temperature, where the enhancement ranged between 15 and 20% higher than that of specimen N-N_{25} at room temperature. Similar findings were identified by Júlio et al. (2006); Momayez et al., 2004), whereas increased compressive strength of post-cast concrete was attributed to improved interfacial properties and increased bond strength. The specimen N-F_{25} showed the highest shear strength due to the presence of FA, which consists of SiO_2 and Al_2O_3 that react with $Ca(OH)_2$ and result in additional C-S–H and fill the pores at the interface and improve the interface of the existing concrete, as discussed by Gao et al. (Ghazy et al., 2022). After 600 °C, the composite specimen N-F_{600} displayed a shear strength of 1.83 MPa, which was 63.5% of its initial shear strength with an increasing ratio of 60.5% than that of N-N_{600}. The thermal stability of FAC at elevated temperatures increases the thermal resistance of the transition zone to high temperatures, which improves the shear strength of specimen N-F than N–N.

On the other hand, specimen N-H_{600} showed more retreating in shear strength after exposure to a temperature of 600 °C, which was 49% of its initial shear strength but stayed higher than that of N-N_{600} by approximately 19%. The results agree with Chen et al. (2023). The difference in the thermal expansion between NSC and HSC contributes to developing microcracks at the interfacial zone, consequently reducing the bond between two concrete parts, as observed by Ghazy et al. (2023). Furthermore, compared with monolithic specimen N_{600}, the shear strength was 1.5 lower and 32.6% higher for specimens N-H_{600} and N-F_{600}, respectively.

3.7 Effect of Fiber Type

For monolithic FSP, the interfacial shear strength was 44.8% and 164.5% higher than that of monolithic N at room temperature and after exposure to a temperature of 600 °C for 90 min. The results agree with Alimrani and Balazs (2020). This is due to the fiber inclusion often made as shear connectors across the interface, resulting in delayed crack propagation and improved resistance to fracture growth (Zanotti et al., 2014). The interfacial shear strength of composite specimens N-FS_{600}, N-FP_{600}, and N-FSP_{600} after exposure to an elevated temperature of 600 °C for 90 min are presented in Fig. 12. The results demonstrated that fiber plays an important role in the interfacial shear strength after exposure to elevated temperature. The composite specimen N-FSP displayed the highest interfacial shear strength with an increasing ratio of 114% compared to specimen N-N_{600}, while the improvement for N-FS_{600} reached 68.8%. The improvement in the interfacial shear strength is due to the use of fibers, which often improve the ability of the concrete to resist fracture growth, reduce overlay shrinkage, and reduce porosity close to the interface, as discussed by Daneshvar et al. (Daneshvar et al., 2022). On the contrary, the incorporation of PP fiber had adverse effects on the shear strength after exposure to elevated temperatures,

where specimen N-FP_{600} displayed the least shear strength; it was 15.6% lower than that of N-N_{600}. The same behavior was observed by Alimrani and Balazs (Alimrani & Balazs, 2020). The deterioration in the interfacial shear strength of specimen N-FP_{600} is due to the melting of PPF at elevated temperatures and the creation of more voids. This resulted in the weakening of the concrete microstructure and the degradation of the adhesive bond properties at the interface.

4 Discussion

For more observations, the interfacial shear strength in this study and previous studies conducted by (Abo Sabah et al. (2019); Haido et al., 2021; Gao et al., 2019; Chen et al., 2023) were presented in Fig. 13 as relative interfacial shear strength, which equals the interfacial shear strength at elevated temperatures related to that at room temperature. The interfacial shear strength was obtained for rough surface conditions in this comparison. From the outcome of the figure, it can be noticed that the concrete compressive strength has a relevant effect on interfacial shear strength, where composite specimens with HSC showed a significant deterioration as compared to those with NSC. This is due to the dense microstructure of HSC, which prevents escaping the vapor water, resulting in more cracks and deteriorating the interfacial bond strength, as observed by Chen et al. (2023). Also, it can be found that the interfacial shear strength improves with including fibers. The fiber bridges the crack and delays crack propagation, leading to increased interfacial shear strength. Moreover, using supplementary cementitious materials can enhance the interfacial shear strength at elevated temperatures.

5 Finite Element Analysis

To simulate and analyze the impact of various time and temperature exposures on the interfacial shear strength of composite specimen N-FSP, a 3D finite element model of a composite push-off specimen was developed. Fig. 14 displays the dimensions of the push-off specimen used to mimic the experimental specimen. Two models were used to predict the impact of temperature on the interfacial shear strength. The first model was the heat transfer model, which was used to determine the temperatures at each node. The second model is the structural model for calculating the interfacial behavior after heating, and it takes the nodal temperatures calculated by the heat transfer model as an input.

The FE of the composite push-off specimen and the boundary condition are depicted in Fig. 14. The heat transfer model for the NSC and FSP parts employs a DC3D8 eight-node linear heat transfer brick. The structural model employs C3D8R bricks with eight nodes, decreased integration, and an hourglass-shaped control element. The reinforcement was simulated using a heat transfer model comprised of a 2-node heat transfer link (DC1D2) and a structural model comprised of a 2-node linear 3D truss (T3D2). NSC and FSP parts were modeled using a 10 mm mesh size. An embedded region model was utilized to simulate the bond between reinforcement and concrete, where concrete was chosen as the host region and reinforcement as the embedded region.

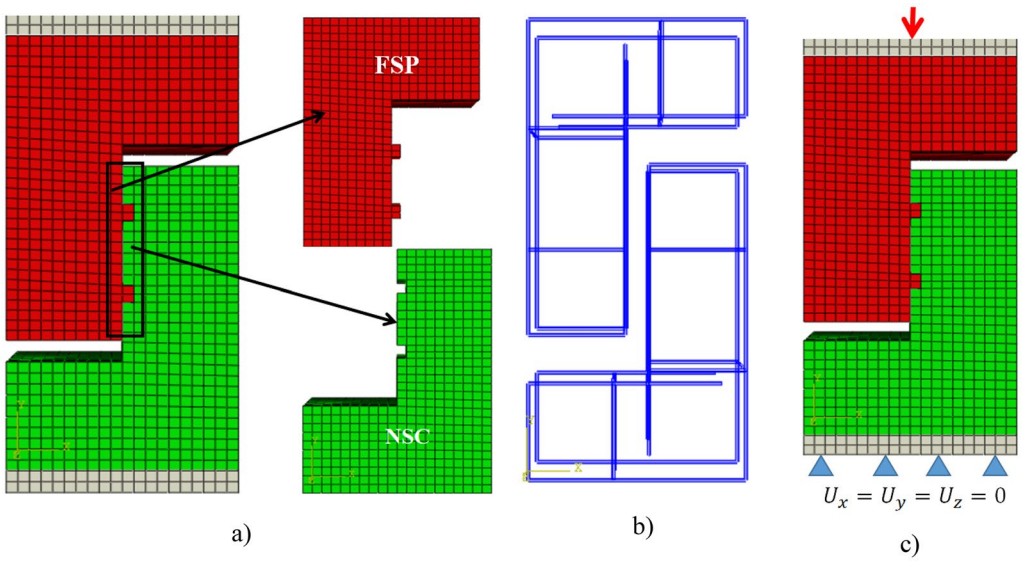

Fig. 14 FE model of composite push-off specimen; **a** concrete parts, **b** reinforcement model, **c** boundary conditions

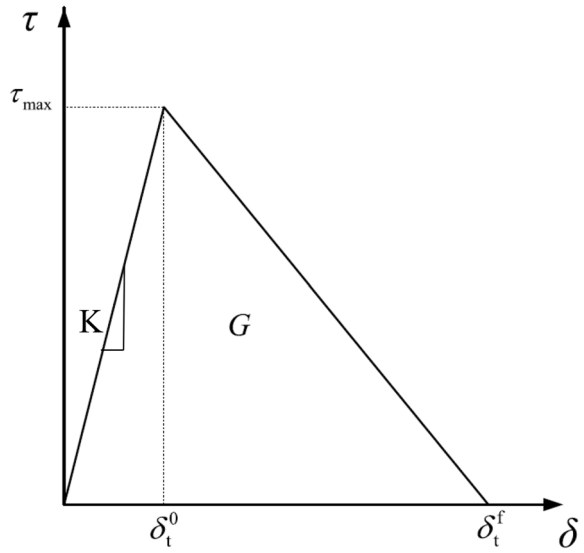

Fig. 15 Cohesive element parameters

5.1 Interfacial Properties

According to experimental results, the failure occurred by crushing NSC; thus, the traction separation model produced by ABAQUS (ABAQUS Manual, 2013) was used to simulate the vertical shear plan. The traction separation model is characterized by the initial stiffness K (elastic linear part), the point of maximum shear τ_{max} and corresponding slip δ_t^0 (point of damage initiation), fracture energy G and failure slip δ_t^f (damage evaluation) as shown in Fig. 15. These parameters were taken from experimental work results (see Table 6). According to Farouk et al. (2022), softening degradation was evaluated using the linear softening law. Furthermore, it is expected that only the horizontal contact surface will experience friction; thus, a penalty tangential model with a friction coefficient of 0.3 was used, according to Zhang et al. (2020c). Thus, in accordance with Farouk et al., the FSP part surface was chosen as the master surface, and the NSC part surface as the salve surface (Farouk et al., 2022).

5.2 Concrete Constitutive Model

As presented in Table 8, the thermal parameters for NSC and FSP needed by the heat transfer model, such as thermal conductivity, specific heat, and density, are obtained from Zalhaf (2022). For the purpose of simulating the nonlinear behavior of NSC and FSP upon exposure to elevated temperature, the concrete damage plasticity model (CDP) was included in the structural model. For FSP, the relationships presented by Li and Kodur (1996) and Lok and Xiao (1998) are used to represent the uniaxial compressive stress–strain curve and the tensile stress–strain curve after exposure to various temperatures, as shown in Fig. 16b, d. Whereas EN1992-1–2 (Eurocode2., 2004) and Massicotte et al. (1990) display the stress–strain curves for NSC under compression and tension, respectively, as in Fig. 16a, c. The modulus of elasticity for NSC and FSP were calculated using correlation $E = 4700\sqrt{f_c}$, where f_c is the concrete compressive strength according to ACI 318–19 (Committee, 2019). The coefficient of deterioration in the modulus of elasticity mentioned by EN 1992–1-2 (Eurocode2., 2004) and Khaliq and Kodur (2011) were used for calculating the deterioration in the modulus of elasticity of NSC and FSP, respectively. Reinforcement rebar temperature impacts on thermal and structural properties were simulated employing EN 1993-1-2 (2005). The steel yield stress and its modulus of elasticity are taken as 360 MPa and 200 GPa, respectively. The Poisson's ratio is taken as 0.2 and 0.3 for concrete and steel materials, respectively, according to EN 1992–1-2 (Eurocode2. 2004). Depending on the experimental observation, no spalling occurred for composite specimen N-FSP at different temperatures and different times up to 120 min, so the spalling is ignored in the FE model.

The shear strength–slip curves obtained from the FE model under different temperatures and different

Table 8 Thermal properties of concrete mixes

Mix ID	Temperature (°C)	Density (kg/m^3)	Thermal conductivity (W.m^{-1}.K^{-1})	Specific heat (J/kg.K)
NSC	25	2300	2	985
	200	2185	1.6	985
	400	2185	1.24	1033
	600	2143	1.15	1149
FAC-(SF + PP)	25	2450	2.94	1060
	200	2425	2.68	1003
	400	2401	1.34	999
	600	2376	0.78	1293

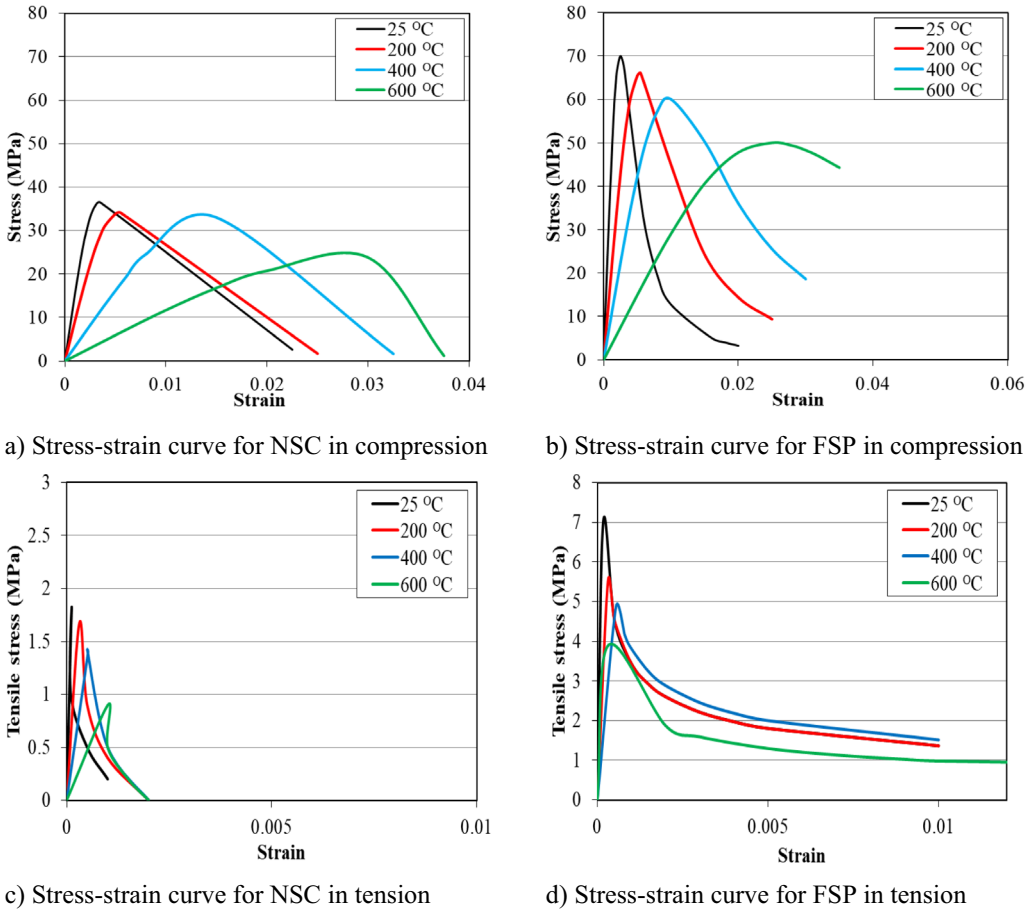

Fig. 16 Stress–strain curves for NSC and FSP after exposure to temperature

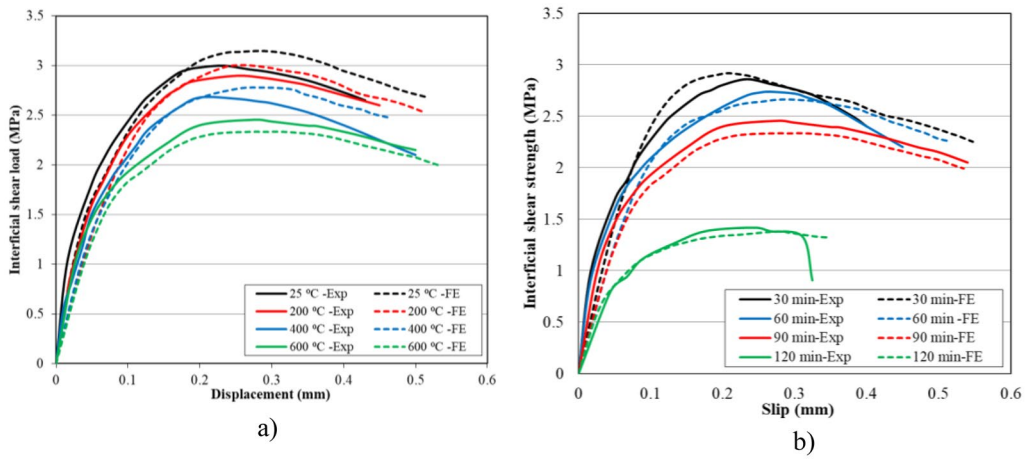

Fig. 17 Predicted shear strength–slip curve versus the experimental results. **a** Different temperatures. **b** Different times of exposure

times of exposure are plotted in Fig. 17 as a comparison with experimental curves. As indicated in the figure, the FE model gave results consistent with experimental results. It demonstrates that using the cohesive model to simulate interfacial properties after high temperatures can improve FE modeling. Table 9 displays the FE

Table 9 Predicted interfacial shear properties

Parameters	Experimental		Finite element		Prediction	
	τ_{Exp}(MPa)	K_{Exp}(N/mm^3)	τ_{FE}(MPa)	K_{FE}(N/mm^3)	K_{FE}/K_{Exp}	τ_{FE}/τ_{Exp}
FSP-N_{25}	3	14.90	3.05	13.65	0.92	1.01
FSP-N_{200}	2.9	11.56	2.85	11.54	0.99	0.98
FSP-N_{400}	2.68	10.68	2.77	9.89	0.93	1.03
FSP-N_{600}	2.44	8.91	2.33	8.63	0.97	0.95
FSP-N_{30min}	2.68	12.25	2.91	13.18	1.07	1.01
FSP-N_{60min}	2.74	11.58	2.65	10.6	0.91	0.97
FSP-N_{90min}	2.45	8.91	2.33	8.63	0.96	0.95
FSP-N_{120min}	1.4	5.88	1.33	5.52	0.94	0.95

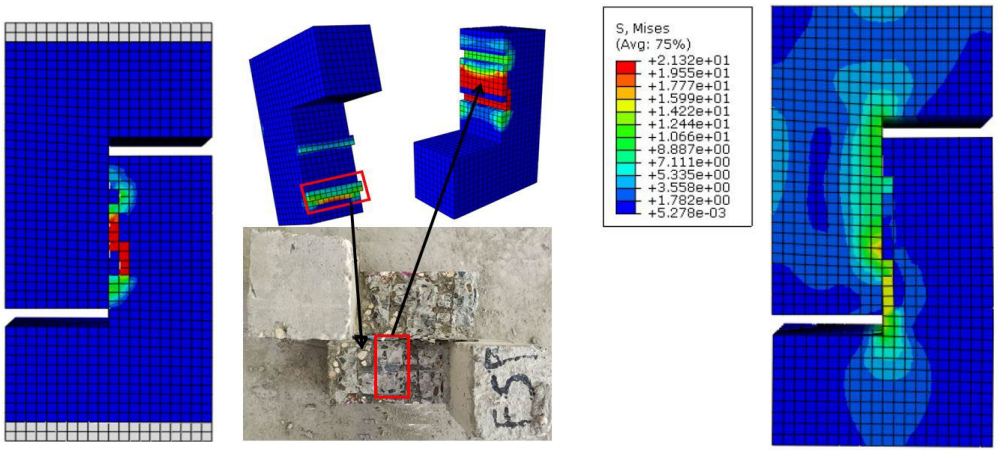

a) Failure pattern b) Stress distribution

Fig. 18 Finite element results

model-derived interfacial shear characteristics. Maximum shear strength predictions have an accuracy of 0.95–1.03. There was also a discrepancy of 0.92–1.07 between the FE stiffness (K_{FE} and the experimental stiffness K_{Exp}.

Fig. 18 shows the failure pattern from the FE model and experimental test. From the Tension damage, it can be observed that the failure occurred by NSC crushing. Furthermore, Fig. 18b demonstrates that the stress concentration is at the shear failure plane.

6 Conclusion

The main aim of this paper was to investigate and analyze the interfacial shear behavior between two layers under the influence of a set of parameters, including temperature, time exposure, concrete type, and fiber type by employing a Z-shape push-off test. The test consists of two parts with different ages: normal strength concrete (NCS) and high-performance concrete (HPC). Finally, a finite element (FE) model was proposed to depict and validate the experimental work. Following is a summary of this study's key findings:

1) Temperature degree and exposure time had adverse effects on the interfacial shear strength.
2) Specimen N-FSP performed better than specimen N–N at different temperature exposures. The interfacial shear strength increased by 24%, 27.7%, 87.5%, and 114% at 25, 200, 400, and 600 °C, respectively.
3) Despite the fracture energy of composite specimen N-FSP increased with increasing temperature, it decreased for specimen N–N. This proves the importance of using SF fiber in improving the ductility of specimens at high temperatures.
4) Fiber types significantly influence interfacial shear strength. Including combined fiber (SF + PPF) improved the interfacial shear strength by 114% compared to composite specimen N–N after exposure to a temperature of 600 °C. In other words, using PPF negatively affected the interfacial shear strength,

which recorded only 84% of composite specimen N–N.

5) Enhancement of interfacial shear strength at elevated temperature achieved using supplementary cementitious material, where composite specimen N-F incorporating 30% FA showed improvement by 60.5% higher than N–N
6) While HSC improves the interfacial shear strength of push-off specimen at room temperature, it showed a significant deterioration after exposure to elevated temperature, which retains 49% of its interfacial strength at room temperature.
7) In general, the monolithic specimens N and FSP had the maximum shear strength compared to the composite specimens.
8) The finite element model of the interfacial shear strength of composite specimen at elevated temperature using cohesive elements gave a good accuracy with test results.

Acknowledgements
The authors acknowledge the contributions of technical staff at the material properties and testing laboratory, Faculty of Engineering, Kafrelsheikh University, Egypt, for providing great assistance and helpful comments in executing the experimental program.

Author contributions
NMZ: participated in writing the research plan, carried out the experimental work, shared in the theoretical work, and participated in writing and reviewing the article. SF: participated in writing and reviewing the article. MHZ: participated in writing the research plan, carried out the experimental work, shared in the theoretical work, and participated in writing and reviewing the article. All authors read and approved the final manuscript.

Funding
Open access funding provided by The Science, Technology & Innovation Funding Authority (STDF) in cooperation with The Egyptian Knowledge Bank (EKB).

Availability of data and materials
The experimental data can be obtained through e-mail communication with the author at Mohammed_hamed@eng.kfs.edu.eg.

Declarations

Competing interests
The authors declare that they have no competing interests.

Received: 10 September 2023 Accepted: 9 December 2023
Published online: 27 March 2024

References

ABAQUS Version 6.13. (2013). Abaqus Analysis User Manual, Dassault Systems, USA. http://130.149.89.49:2080/v6.13/index.html. Accessed 5 Nov 2010

Abo Sabah, S. H., Zainal, N. L., Muhamad Bunnori, N., Megat Johari, M. A., & Hassan, M. H. (2019). Interfacial behavior between normal substrate and green ultra-high-performance fiber-reinforced concrete under elevated temperatures. *Structural Concrete, 20*(6), 1896–1908. https://doi.org/10.1002/suco.201900152

ACI Committee. (2019). Building code requirements for structural concrete (ACI 318-19) and commentary. American Concrete Institute

Ahmad, S., Bhargava, P., Chourasia, A., & Usmani, A. (2020). Effect of elevated temperatures on the shear-friction behaviour of concrete: Experimental and analytical study. *Engineering Structures, 225*, 111305.

Algourdin, N., Pliya, P., Beaucour, A.-L., et al. (2020). Influence of polypropylene and steel fibres on thermal spalling and physical-mechanical properties of concrete under different heating rates. *Construction and Building Materials*. https://doi.org/10.1016/j.conbuildmat.2020.119690

Alimrani, N. S., & Balazs, G. L. (2020). Investigations of direct shear of one-year old SFRC after exposed to elevated temperatures. *Construction and Building Materials, 254*, 119308.

ASTM C29/C29M-07. (2010). Standard test method for bulk density ("Unit Weight") and voids in aggregate. ASTM International, West Conshohocken, PA, USA.

ASTM-C127–01. (2017). Standard test method for density, relative density (Specific Gravity), and absorption of coarse aggregate. ASTM International, West Conshohocken, PA, USA.

ASTM C128–01. (2017). Standard test method for density, relative density (Specific Gravity), and absorption of fine aggregate. ASTM International, West Conshohocken, PA, USA.

Babalola, O. E., Awoyera, P. O., Le, D. H., & Romero, L. B. (2021). A review of residual strength properties of normal and high strength concrete exposed to elevated temperatures: Impact of materials modification on behaviour of concrete composite. *Construction and Building Materials, 296*, 123448.

Baloch, W. L., Siad, H., Lachemi, M., & Sahmaran, M. (2023). Effect of high temperatures on hot-bonded SCC/ECC and SCC/UHPC composite systems. *Construction and Building Materials, 369*, 130507.

Bentz, D. P., De la Varga, I., Muñoz, J. F., Spragg, R. P., Graybeal, B. A., Hussey, D. S., & LaManna, J. M. (2018). Influence of substrate moisture state and roughness on interface microstructure and bond strength: Slant shear vs. pull-off testing. *Cement and Concrete Composites, 87*, 63–72. https://doi.org/10.1016/j.cemconcomp.2017.12.005

Beushausen, H. (2010). The influence of concrete substrate preparation on overlay bond strength. *Magazine of Concrete Research, 62*(11), 845–852.

BS EN 12390–6. (2009). Testing hardened concrete. Tensile splitting strength of test specimens. British Standards Institution, London, UK.

BS EN 12390-3. (2019). Testing hardened concrete. Compressive strength of test specimens. British Standards Institution, London, UK

CEB-FIP, Model Code. (2010). International federation for structural concrete, Lausanne, Switzerland, 2010

Chen, Z., Xiao, J., Ding, T., & Liu, B. (2023). Push-off test on concrete-concrete interface with different types of concrete after elevated temperatures. *Construction and Building Materials, 377*, 131157.

Daneshvar, D., Behnood, A., & Robisson, A. (2022). Interfacial bond in concrete-to-concrete composites: A review. *Construction and Building Materials, 359*, 129195.

EN 1993-1-2. (2005). Eurocode 3: design of steel structures-part 1–2: general rules-structural fire design. European Committee for Standardization, Brussels

Eurocode 2. (2004). Design of concrete structures, Part 1–2: General rules-structural fire design. ENV 1992–1–2/ UK: CEN: European Committee for Standardization

Farouk, A. I. B., Zhu, J., & Yuhui, G. (2022). Finite element analysis of the shear performance of box-groove interface of ultra-high-performance concrete (UHPC)-normal strength concrete (NSC) composite girder. *Innovative Infrastructure Solutions, 7*(3), 212.

Feng, S., Xiao, H., & Geng, J. (2020). Bond strength between concrete substrate and repair mortar: Effect of fibre stiffness and substrate surface roughness. *Cement and Concrete Composites, 114*, 103746.

Gao, S., Zhao, X., Qiao, J., Guo, Y., & Hu, G. (2019). Study on the bonding properties of Engineered Cementitious Composites (ECC) and existing concrete exposed to high temperature. *Construction and Building Materials, 196*, 330–344. https://doi.org/10.1016/j.conbuildmat.2018.11.136

Ghazy, M. F., Abd Elaty, M. A., & Zalhaf, N. M. (2022). Mechanical properties of HPC incorporating fly ash and ground granulated blast furnace slag after exposure to high temperatures. *Periodica Polytechnica Civil Engineering, 66*(3), 761–774. https://doi.org/10.3311/PPci.19751

Ghazy, M. F., Abd Elaty, M. A., & Zalhaf, N. M. (2023). Performance of normal strength concrete slab strengthened with high-performance concrete

after exposure to elevated temperature. *Fire Technology*. https://doi.org/10.1007/s10694-023-01439-y
Haido, J. H., Tayeh, B. A., Majeed, S. S., & Karpuzcu, M. (2021). Effect of high temperature on the mechanical properties of basalt fibre self-compacting concrete as an overlay material. *Construction and Building Materials, 268*, 121725. https://doi.org/10.1016/j.conbuildmat.2020.121725
Jiang, H., Dong, X., Fang, Z., Xiao, J., & Chen, Y. (2020). Experimental study on shear behavior of a Uhpc connection between adjacent precast prestressed concrete voided beams. *Journal of Bridge Engineering, 25*, 04020106. https://doi.org/10.1061/(ASCE)BE.1943-5592.0001644
Jiang, H., Shao, T., Fang, Z., Xiao, J., & Hu, Z. (2021). Shear-friction behavior of grooved construction joints between a precast uhpc girder and a cast-in-place concrete slab. *Engineering Structures, 228*, 111610. https://doi.org/10.1016/j.engstruct.2020.111610
Julio, E. N., Branco, F. A., & Silva, V. D. (2004). Concrete-to-concrete bond strength. Influence of the roughness of the substrate surface. *Construction and Building Materials, 18*(9), 675–681.
Júlio, E. N., Branco, F. A., Silva, V. D., & Lourenço, J. F. (2006). Influence of added concrete compressive strength on adhesion to an existing concrete substrate. *Building and Environment, 41*(12), 1934–1939. https://doi.org/10.1016/j.buildenv.2005.06.023
Khaliq, W., & Kodur, V. (2011). Thermal and mechanical properties of fiber reinforced high performance self-consolidating concrete at elevated temperatures. *Cement and Concrete Research, 41*(11), 1112–1122. https://doi.org/10.1016/j.cemconres.2011.06.012
Khaliq, W., & Kodur, V. (2013). Behavior of high strength fly ash concrete columns under fire conditions. *Mater and Struct., 46*, 857–867. https://doi.org/10.1617/s11527-012-9938-7
Li, H., & Liu, G. (2016). Tensile properties of hybrid fiber-reinforced reactive powder concrete after exposure to elevated temperatures. *International Journal of Concrete Structures and Materials., 10*(1), 29–37. https://doi.org/10.1007/s40069-016-0125-z
Lie, T. T., & Kodur, V. K. R. (1996). Thermal and mechanical properties of steel-fibre-reinforced concrete at elevated temperatures. *Canadian Journal of Civil Engineering, 23*(2), 511–517.
Lok, T. S., & Xiao, J. R. (1998). Tensile behaviour and moment–curvature relationship of steel fibre reinforced concrete. *Magazine of Concrete Research, 50*(4), 359–368.
Ma, Q., Guo, R., Zhao, Z., Lin, Z., & He, K. (2015). Mechanical properties of concrete at high temperature—a review. *Construction and Building Materials, 93*, 371–383. https://doi.org/10.1016/j.conbuildmat.2015.05.131
Mansour, W., & Fayed, S. (2021). Effect of interfacial surface preparation technique on bond characteristics of both NSC-UHPFRC and NSC-NSC composites. *Structures, 29*, 147–166.
Massicotte, B., Elwi, A. E., & MacGregor, J. G. (1990). Tension stiffening model for planar reinforced concrete members. *ASCE Journal of Structural Engineering, 116*(11), 3039–3058.
Mathews, M. E., Anand, N., Lubloy, E., & Kiran, T. (2021). Effect of elevated temperature on interfacial shear transfer capacity of self-compacting concrete. *Case Studies in Construction Materials, 15*, e00753.
Momayez, A., Ramezanianpour, A. A., Rajaie, H., & Ehsani, M. R. (2004). Bi-surface shear test for evaluating bond between existing and new concrete. *Materials Journal, 101*(2), 99–106. https://doi.org/10.14359/13045
Park, J. K., & Kim, M. O. (2021). The effect of different exposure conditions on the pull-off strength of various epoxy resins. *Journal of Building Engineering, 38*, 102223. https://doi.org/10.1016/j.jobe.2021.102223
Poon, C.-S., Azhar, S., Anson, M., et al. (2001). Comparison of the strength and durability performance of normal-and high-strength pozzolanic concretes at elevated temperatures. *Cement and Concrete Research, 31*(9), 1291–1300. https://doi.org/10.1016/S0008-8846(01)00580-4
Santos, D. S., Santos, P. M., & Dias-da-Costa, D. (2012). Effect of surface preparation and bonding agent on the concrete-to-concrete interface strength. *Construction and Building Materials, 37*, 102–110.
Santos, P. M., & Julio, E. N. (2007). Correlation between concrete-to-concrete bond strength and the roughness of the substrate surface. *Construction and Building Materials, 21*(8), 1688–1695. https://doi.org/10.1016/j.conbuildmat.2006.05.044
Schneider, U. (1988). Concrete at high temperatures—a general review. *Fire Safety Journal, 13*(1), 55–68.
Shang, X. Y., Xu, F. Z., Yu, J. T., Li, L. Z., & Lu, Z. D. (2021). Study on the interfacial shear performance between engineered cementitious composites and concrete after being subjected to high temperatures. *Journal of Building Engineering, 44*, 103328. https://doi.org/10.1016/j.jobe.2021.103328
Sun, J., Fan, J., Chen, A., & Yuan, L. (2022). Interfacial properties between autoclaved aerated concrete and concrete after high temperature. *Journal of Building Engineering, 60*, 105213. https://doi.org/10.1016/j.jobe.2022.105213
Tayeh, B. A., Abu Bakar, B. H., & Megat Johari, M. A. (2013). Characterization of the interfacial bond between old concrete substrate and ultra high performance fiber concrete repair composite. *Materials and Structures, 46*, 743–753.
Valikhani, A., Jahromi, A. J., Mantawy, I. M., & Azizinamini, A. (2021). Effect of mechanical connectors on interface shear strength between concrete substrates and UHPC: Experimental and numerical studies and proposed design equation. *Construction and Building Materials, 267*, 120587. https://doi.org/10.1016/j.conbuildmat.2020.120587
Yang, J., Xia, J., Cheng, C., Wang, J., Zhang, J., & Wang, G. (2022). Research on the bonding performance of UHPC–NC interfaces with different sizes of grooves. *Frontiers in Materials, 9*, 859717.
Zalhaf NM. (2022). "Performance of strengthened concrete with high performance concrete under fire" PhD thesis, Department of Structural Engineering, Faculty of Engineering, Tanta University, Tanta, Egypt, 197 Pp.
Zanotti, C., Banthia, N., & Plizzari, G. (2014). A study of some factors affecting bond in cementitious fiber reinforced repairs. *Cement and Concrete Research, 63*, 117–126. https://doi.org/10.1016/j.cemconres.2014.05.008
Zanotti, C., Rostagno, G., & Tingley, B. (2018). Further evidence of interfacial adhesive bond strength enhancement through fiber reinforcement in repairs. *Construction and Building Materials, 160*, 775–785.
Zhang, Y., Zhu, P., Liao, Z., & Wang, L. (2020a). Interfacial bond properties between normal strength concrete substrate and ultra-high performance concrete as a repair material. *Construction and Building Materials, 235*, 117431. https://doi.org/10.1016/j.conbuildmat.2019.117431
Zhang, Y., Zhu, P., Wang, X., & Wu, J. (2020b). Shear Properties of the interface between ultra-high performance concrete and normal strength concrete. *Construction and Building Materials, 248*, 118455. https://doi.org/10.1016/j.conbuildmat.2020.118455

Publisher's Note

Nagat M. Zalhaf is an assistant professors in the Department of Civil Engineering, Faculty of Engineering, Kafrelsheikh University, Kafrelsheikh City, Egypt.

Sabry Fayed is an associate professor in the Department of Civil Engineering, Faculty of Engineering, Kafrelsheikh University, Kafrelsheikh, Egypt.

Mohamed H. Zakaria is an assistant professors in the Department of Civil Engineering, Faculty of Engineering, Kafrelsheikh University, Kafrelsheikh City, Egypt.